Lumped-Element Dynamic Electro-Thermal model of a superconducting magnet

E. Ravaioli[a,b], B. Auchmann[a], M. Maciejewski[a,c], H.H.J. ten Kate[a,b], and A.P. Verweij[a]

[a] *CERN, the European Center for Nuclear Research, POB Geneva 23, 1211, Switzerland*
[b] *University of Twente, Enschede, The Netherlands*
[c] *Institute of Automatic Control, Technical University of Łódź, 18/22 Stefanowskiego St., Poland*

Abstract

Modeling accurately electro-thermal transients occurring in a superconducting magnet is challenging. The behavior of the magnet is the result of complex phenomena occurring in distinct physical domains (electrical, magnetic and thermal) at very different spatial and time scales. Combined multi-domain effects significantly affect the dynamic behavior of the system and are to be taken into account in a coherent and consistent model.

A new methodology for developing a Lumped-Element Dynamic Electro-Thermal (LEDET) model of a superconducting magnet is presented. This model includes non-linear dynamic effects such as the dependence of the magnet's differential self-inductance on the presence of inter-filament and inter-strand coupling currents in the conductor. These effects are usually not taken into account because superconducting magnets are primarily operated in stationary conditions. However, they often have significant impact on magnet performance, particularly when the magnet is subject to high ramp rates.

Following the LEDET method, the complex interdependence between the electro-magnetic and thermal domains can be modeled with three sub-networks of lumped-elements, reproducing the electrical transient in the main magnet circuit, the thermal transient in the coil cross-section, and the electro-magnetic transient of the inter-filament and inter-strand coupling currents in the coil's superconductor. The same simulation environment can simultaneously model macroscopic electrical transients and phenomena at the level of superconducting strands.

Preprint submitted to Cryogenics *September 18, 2015*

The model developed is a very useful tool for reproducing and predicting the performance of conventional quench protection systems based on energy extraction and quench heaters, and of the innovative CLIQ protection system as well.

Keywords: Circuit modeling, Coupling losses, Quench protection, Simulation, Superconducting coil

---

1. Introduction

The presence of interdependent, non-linear, multi-domain and multi-scale phenomena make the modeling of superconducting circuits particularly challenging.

The interest in software capable to reproduce and predict the electro-magnetic and thermal transients occurring in superconducting coils subject to high current changes has been growing. The influence of transitory loss on the magnet protection after a transition to the normal state needs to be analyzed more carefully when designing new-generation, high magnetic-field, high energy-density magnets. Furthermore, the recent invention of CLIQ (Coupling-Loss Induced Quench) protection system [1] made mandatory the development of a reliable tool for modeling transitory loss and non-linear effects.

An new Lumped-Element Dynamic Electro-Thermal (LEDET) model of a superconducting magnet is presented here. This technique allows simulating non-linear dynamic effects such as the dependence of the magnet's differential self-inductance on the presence of local inter-filament and inter-strand coupling currents in the conductor. These effects often have significant impact on magnet performance and protection, particularly when the magnet is subject to high ramp rates.

2. Dynamic electro-thermal model

The proposed LEDET method is used to model the behavior of a superconducting magnet by means of a network of lumped-elements. It includes purely electrical components, a 2D thermal model of the coil cross-section, and a model of the coupling currents in the coil and their influence on the electrical components.

2.1. Lumped-element modeling

Finite-element modeling (FEM) is an advanced and powerful computational method of solving boundary-value problems on the basis of domain discretization into a finite number of elements. Non-linear behavior in superconducting cables can be successfully reproduced by means of such software [2, 3]. However, the computational effort required to obtain accurate results is usually high, which makes FEM application inefficient due to the long simulation time.

An alternative approach consists in modeling the dynamic behavior of a superconducting magnet by means of a network of non-linear lumped-elements, which is then solved with an in-house or commercial network solver, such as Simulink, PSpice, SPICE, or Simplorer. In fact, in many practical cases the electro-magnetic and thermal dynamics of a superconducting magnet can be effectively reproduced with a limited number of differential-algebraic equations. This technique requires a deep understanding of the phenomena occurring in the coil strands and cables, which significantly influence the system dynamics. Once properly implemented it renders a significant reduction in CPU time for solving the model with respect to FEM.

The same simulation environment can simultaneously model macroscopic electrical transients and phenomena occurring at the level of superconducting strands. Thus, the flexibility of the model is greatly improved.

2.2. LEDET in a nutshell

Figure 1 shows a schematic representation of a purely electrical model and the interaction between its components, subdivided into energy sources, sinks, or storage elements. The energy provided by the power source (PS) is stored in capacitive (C) and inductive (L) elements, and dissipated in resistive components (R), such as resistors, diodes, or switches. The model is a closed system with only two energy-exchange interfaces with the exterior: energy exchanges with an infinite source, representing the main electric network (EN), and energy output to an infinite sink, representing the room-temperature environment (RT).

An electro-thermal model includes an electrical sub-system similar to the previous example interacting with a thermal sub-system [4, 5, 6]. For instance, the thermal network used by the LEDET model is described in section 4. Since the transient occurring in one domain influences the other, and vice versa, the two subsystems can be solved simultaneously by

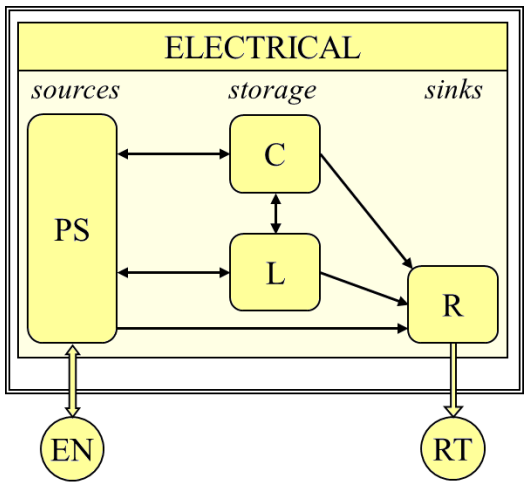

Figure 1: Representation of the energy exchanges occurring in a purely electrical model.

the simulation software. A typical example of electro-thermal transient is the generation of ohmic loss, whose occurrence builds a voltage across the conductor, which affects the electrical domain, and enhances its temperature, which affects the thermal domain.

The energy exchanges in a model composed of an electrical and a thermal sub-system are represented in figure 2. Within the thermal domain, energy is stored in heat-capacitance elements (C_{th}), which can exchange energy with each others (P_{ex}). Energy transferred to infinite heat sinks is dissipated and lost to the system. This is the case, for instance, of the heat delivered to a helium bath (HE) surrounding a superconducting coil (P_{He}).

The electrical and thermal sub-systems exchange energy through components simulating ohmic loss internal to the conductor ($R_C \rightarrow P_{ohm}$). To satisfy the overall energy balance in the entire electro-thermal system, the energy dissipated in the electrical components R_C must equal the input energy to the thermal sub-system through the components P_{ohm}.

Additional energy input can be included in the thermal sub-system to account for other loss sources. These contributions are often added as heat inputs from sources external to the electro-thermal system. This approach is satisfactory only in the case the physical phenomena causing the loss are not related to the magnet system considered, as in the case of radiation or beam loss. Instead, coupling-loss effects cannot be treated as an external, independent heat source since by definition it is generated by an

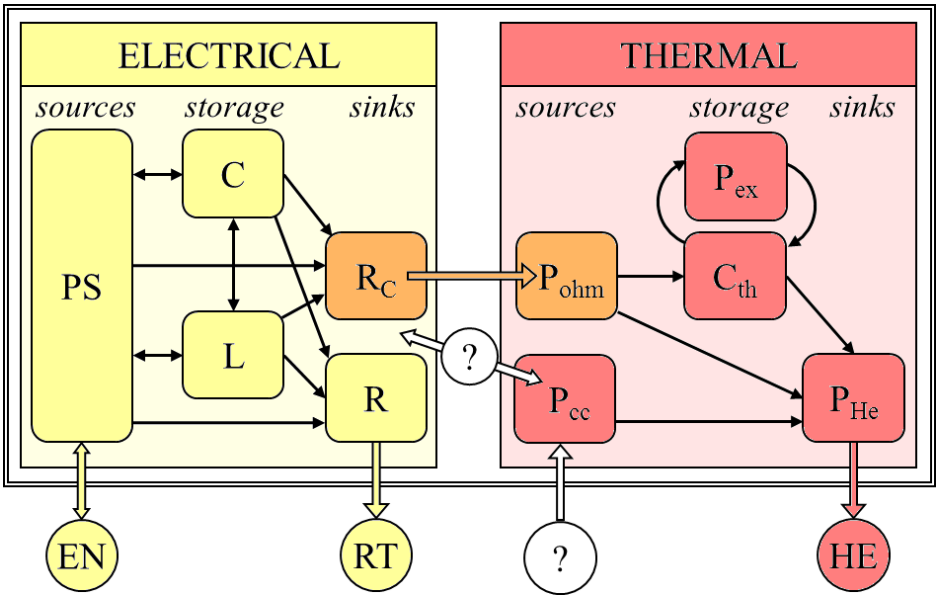

Figure 2: Representation of the energy exchanges occurring in a conventional electro-thermal model. The two main shortcomings of this approach are indicated by question marks.

electro-magnetic interaction between the magnet's field and its conductor.

In fact, a variation in the magnet transport current determines a change of the magnetic field applied to its conductor, dB_a/dt [Ts^{-1}], which in turn results in the generation of an induced magnetic field B_{if} [T] opposing the applied magnetic-field change [7, 8]. Thus, during electro-magnetic transients part of the magnetic energy stored in the superconducting coil does not contribute to the generation of the main coil's magnetic field, but to the development of local induced magnetic fields, that cause currents flowing between superconducting filaments. In a cable with multiple strands, similar currents are also generated between strands. These coupling currents, developed with a characteristic time constant, flow through the strand matrix and through strand-to-strand contact resistances and both result in local ohmic losses, which are called inter-filament and inter-strand coupling loss, respectively [9, 10, 8]. The resulting total magnetic field is the sum of the applied and induced magnetic fields,

$$B_t = B_a + B_{if}. \qquad [T] \quad (1)$$

Many existing electro-thermal models are inadequate to correctly simulate

the effect of local coupling currents and consequently coupling loss in the magnet system. Their shortcomings, schematically illustrated in figure 2, are twofold. Firstly, they do not correctly reproduce the energy flows in the magnet system. In fact, in reality the energy developed as coupling loss P_{cc} [J] and appearing as a heat source in the thermal sub-system does not come from an external system, but is subtracted from the magnet stored energy. Ultimately, this loss is provided by the main power source. This is also the physical background allowing the measurement of coupling loss by calculating the time integral of the energy provided by the power source during a current cycle, $\oint U_{\mathrm{ps}} I_{\mathrm{M}} dt$ [J], with U_{ps} [V] the voltage across the power source and I_{M} [A] the magnet transport current. Secondly, the dependence of the magnet differential self-inductance on the coupling currents developed in the coil is disregarded. Since local coupling currents change the local magnetic flux in the conductor Φ [Tm^2], they obviously have an influence on the effective differential self-inductance of the magnet, $L_{\mathrm{d}}{=}d\Phi/dI_{\mathrm{M}}$ [H].

With the proposed LEDET approach, represented in figure 3, a third coupling-current sub-system is included in the magnet model to describe the energy exchange between the electrical and thermal sub-systems through local coupling currents. The amount of energy subtracted from the magnet and determining a change of its differential self-inductance is the input to the coupling sub-system ($\mathrm{M_{cc}}{\leftrightarrow}\mathrm{M_{cc}}$). This is the stored magnetic energy which maintains the coupling currents flowing ($\mathrm{L_{cc}}$). Part of this energy is returned to the electrical sub-system, and another part is lost and constitutes the heat generated in the conductor due to coupling loss ($\mathrm{R_{cc}}{\rightarrow}\mathrm{P_{cc}}$).

Following the LEDET method, the complex interdependence between the electro-magnetic and thermal domains can be represented with three sub-networks of lumped-elements, reproducing the electrical transient in the main magnet circuit, the thermal transient in the coil cross-section, and the electro-magnetic transient of the inter-filament and inter-strand coupling currents in the coil's superconductor, respectively. The software solves the three sub-networks simultaneously treating them as coupled networks.

A simulation software called TALES (Transient Analysis with Lumped-Elements of Superconductors), was recently developed in order to automatize the process of developing, editing, and running LEDET models in a fast and convenient way [1, 11, 12]. The simulation results have been routinely validated against experimental results [1, 13, 14, 15, 16, 17, 18, 19, 20, 21, 22].

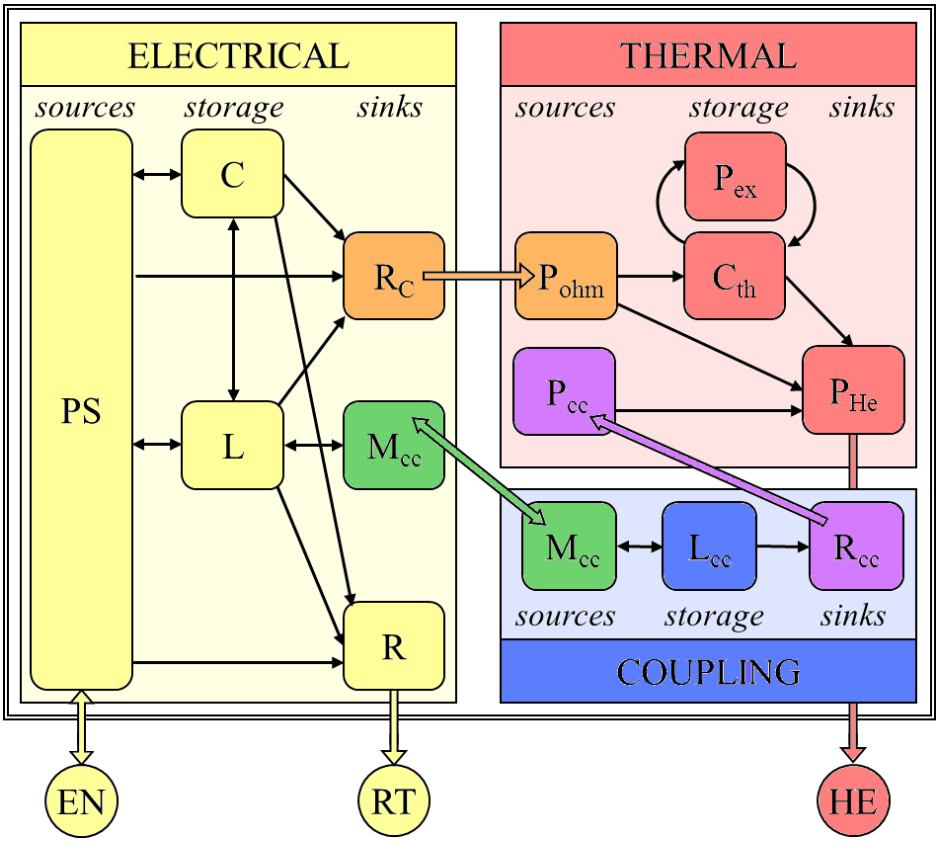

Figure 3: Representation of the energy exchanges occurring in a LEDET model. Elements pertaining to one sub-network are represented in yellow (electrical), red (thermal), and blue (coupling). Elements pertaining to two different sub-networks are represented in orange (electrical-thermal), green (electrical-coupling), and purple (coupling-thermal).

3. Electrical sub-network

The LEDET electrical sub-network contains conventional electrical lumped-elements such as voltage and current sources, self- and mutual inductances, resistors, capacitors, diodes, thyristors, switches, and ground connections.

The parameters of the electrical elements can vary with temperature, magnetic field, transport current, or other relevant physical properties, such as electrical resistivity, heat capacity, and thermal conductance.

A superconducting magnet is represented as a series connection of N_{E} electrical elements. Each element e is composed of a self-inductance L_{e} [H], mutually coupled to the other magnet self-inductances, and a resistor R_{e} [Ω], which is non-zero only in the case of a transition to the normal state. If the magnet is surrounded by an iron yoke, L_{e} decreases with transport current due to iron yoke saturation.

A reasonable choice for the number of electrical elements N_{E} can be the number of poles in a multi-pole magnet, or the number of layers in a solenoid magnet. In conventional applications the same transport current I_{e} [A] flows in the coil of each electrical element. However, after a CLIQ discharge different current changes are introduced in the various coil sections [1].

4. Thermal sub-network

The method for describing a thermal problem with analogous electrical equations and then solving it in the electrical domain is well known in the literature [4, 5, 6]. A thermal system can be represented as an electrical network where any current flowing in a branch of the circuit is equivalent to a heat flow and the potential of any node is equivalent to a temperature.

The thermal sub-network is composed of N_{B} thermal blocks. Each block corresponds to a certain volume of conductor, usually comprising one or a few coil turns. The physical and magnetic properties in each block are assumed homogeneous and are averaged over the block volume. The thermal balance in each block b reads

$$P_{\mathrm{if,b}} + P_{\mathrm{is,b}} + P_{\mathrm{ohm,b}} + P_{\mathrm{ex,b}} + P_{\mathrm{He,b}} = C_{\mathrm{b}}(T_{\mathrm{b}}) \frac{d[(T_{\mathrm{b}} - T_{\mathrm{He}})]}{dt}, \ \ [\mathrm{W}] \quad (2)$$

where $P_{\mathrm{if,b}}$, $P_{\mathrm{is,b}}$, and $P_{\mathrm{ohm,b}}$ [W] are the heat sources corresponding to the inter-filament and inter-strand coupling loss and ohmic loss in block b,

respectively, $P_{\mathrm{ex,b}}$ [W] is the heat exchanged with other blocks, $P_{\mathrm{He,b}}$ [W] is the heat flow to the helium bath, C_{b} [JK^{-1}] is the thermal capacity of b, T_{b} [K] is its average temperature, and T_{He} [K] is the temperature of the helium bath surrounding the magnet, assumed constant. The calculation of $P_{\mathrm{if,b}}$ and $P_{\mathrm{is,b}}$ will be treated in sections 5.1 and 5.2, respectively.

In a conductor composed of a superconductor and a stabilizer, the ohmic loss can be calculated as

$$P_{\mathrm{ohm,b}} = R_{\mathrm{b}} I_{\mathrm{e(b)}}^2 = \frac{\rho_{\mathrm{b}}(T_{\mathrm{b}}, B_{\mathrm{t,b}}) N_{\mathrm{c,b}} l_{\mathrm{b}}}{S_{\mathrm{b}} f_{\mathrm{st,b}}} I_{\mathrm{e(b)}}^2 q_{\mathrm{b}}, \qquad [\mathrm{W}] \quad (3)$$

where R_{b} [Ω] is the electrical resistance of block b, $I_{\mathrm{e(b)}}$ [A] is the current flowing in the electrical element e where b is located, ρ_{b} [Ωm] is the average resistivity of the stabilizer in the block strands, $B_{\mathrm{t,b}}$ [T] is the average absolute value of the total magnetic field in block b, defined in equation 1, $N_{\mathrm{c,b}}$ is the number of conductors (coil turns) in block b, l_{b} [m] is the conductor length, S_{b} [m^2] is the conductor cross-section, including its insulation and impregnation, $f_{\mathrm{st,b}}$ is the volumetric fraction of stabilizer, and q_{b} is either 0 or 1 if block b is in the superconducting or in the normal state, respectively.

The parameter q_{b} in equation 3 is set to 1 any time the T_{b} is larger than the current-sharing temperature in the strand with the highest magnetic field located in block b. In fact, due to the transposition of the cable strands, each strand occupies the highest magnetic-field position within the cable cross-section twice every strand twist-pitch length. The transition from the superconducting to the normal state is considered to be instantaneous.

The approach followed for the calculation of the heat diffusion between adjacent blocks is schematized in figure 4a. By assuming that the temperature is uniform in the conductor and in its insulation layer, and that heat diffusion occurs only in the direction perpendicular to the insulation layers, the heat exchanged by block b with other blocks can be approximated as

$$P_{\mathrm{ex,b}} = -\sum_{h=1}^{N_{\mathrm{bh}}} \frac{k_{\mathrm{b}}(T_{\mathrm{b}}) k_{\mathrm{h}}(T_{\mathrm{h}})}{s_{\mathrm{h}} k_{\mathrm{b}}(T_{\mathrm{b}}) + s_{\mathrm{b}} k_{\mathrm{h}}(T_{\mathrm{h}})} A_{\mathrm{b,h}} (T_{\mathrm{b}} - T_{\mathrm{h}}), \qquad [\mathrm{W}] \quad (4)$$

where N_{bh} is the number of blocks that exchange heat with b, $A_{\mathrm{b,h}}$ [m^2] is the contact area between blocks b and h, s_{b} and s_{h} [m] are the insulation thicknesses of the conductor in blocks b and h, k_{b} and k_{h} [Wm^{-1}K^{-1}] are the thermal conductivities of the insulation material in blocks b and h, and

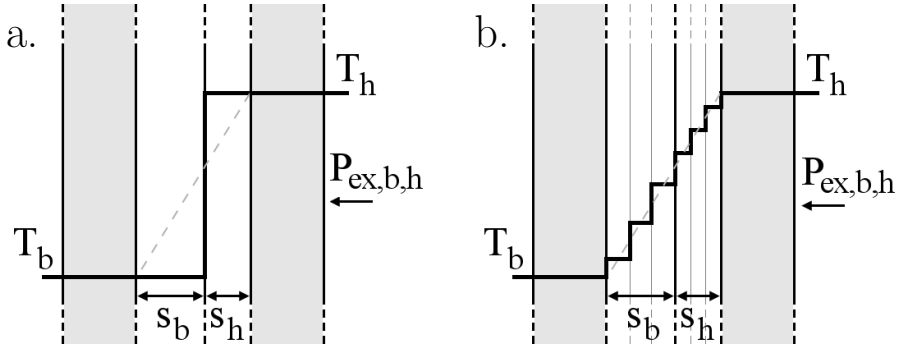

Figure 4: Model adopted to calculate the heat diffusion between blocks b and h. Temperature profile along the direction perpendicular to the insulation layer. a. Simplified one-layer approach. b. Multi-layer approach.

T_{h} [K] is the average temperature in block h. Note that the thermal barrier due to the conductor material is neglected because it is much smaller than that due to the insulation layer.

This simplified one-layer approach is usually satisfactory when simulating electro-thermal transients in superconducting coils since the contribution of thermal diffusion is less than about 10% of the ohmic power generated in the conductor during the magnet discharge. However, if required the model can be improved by considering that the conductor insulation is composed of multiple regions, each with different temperature and hence different thermal conductivity, as shown in figure 4b.

The heat dissipated into the helium bath can be calculated as

$$P_{\mathrm{He,b}} = -h_{\mathrm{He,b}}(T_{\mathrm{b}}, T_{\mathrm{He}}) A_{\mathrm{b,He}} (T_{\mathrm{b}} - T_{\mathrm{He}}), \qquad [\mathrm{W}] \quad (5)$$

where $h_{\mathrm{He,b}}$ [$\mathrm{Wm^{-2}K^{-1}}$] is the heat transfer coefficient between block b and the helium bath surrounding the magnet and $A_{\mathrm{b,He}}$ [$\mathrm{m^2}$] is the contact area between b and the helium bath.

The total thermal capacity of block b is the sum of the thermal capacities of the $N_{\mathrm{m,b}}$ materials composing its volume, including superconductor, stabilizer, insulation, and impregnation:

$$C_{\mathrm{b}} = \sum_{m=1}^{N_{\mathrm{m,b}}} C_{\mathrm{m,b}}(T_{\mathrm{b}}) = V_{\mathrm{b}} \sum_{m=1}^{N_{\mathrm{m,b}}} [c_{\mathrm{m,b}}(T_{\mathrm{b}}) f_{\mathrm{m,b}}], \qquad [\mathrm{JK^{-1}}] \quad (6)$$

where $V_{\mathrm{b}} = S_{\mathrm{b}} l_{\mathrm{b}}$ [$\mathrm{m^3}$] is the volume of block b, $C_{\mathrm{m,b}}$ [$\mathrm{JK^{-1}}$] the heat capacity

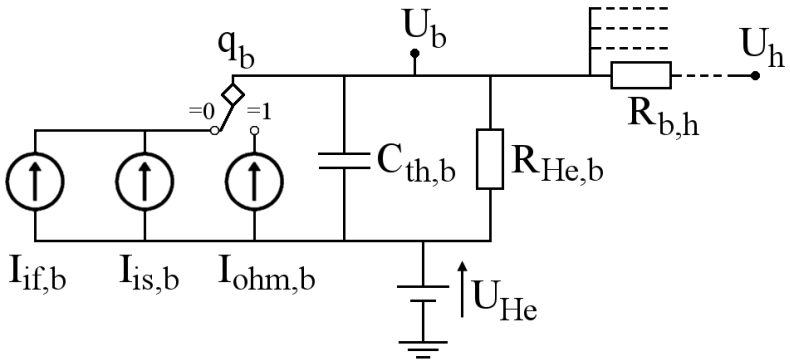

Figure 5: Equivalent LEDET sub-network modeling the thermal behavior of block b.

of material m, $c_{\mathrm{m,b}}$ [$\mathrm{JK^{-1}m^{-3}}$] the specific heat of material m, and $f_{\mathrm{m,b}}$ is the volumetric fraction of material m in block b.

The thermal system described by equations 2-5 can be represented by the analogous electrical circuit shown in figure 5. The characteristic equations of this electrical circuit correctly reproduce the behavior of the thermal system if the equivalent parameters are defined as shown in table 1.

The interaction between the thermal and electrical sub-networks is twofold. Firstly, the ohmic loss $P_{\mathrm{ohm,b}}$ in block b depends on the current $I_{\mathrm{e(b)}}$ flowing in the electrical element e where block b is located. Secondly, the resistance R_{e} of each electrical element e is the sum of the resistances in the $N_{\mathrm{B,e}}$ blocks contained in e,

$$R_{\mathrm{e}} = \sum_{b \in e} R_{\mathrm{b}} = \sum_{b \in e} \frac{\rho_{\mathrm{b}}(T_{\mathrm{b}}, B_{\mathrm{t,b}}) l_{\mathrm{b}}}{S_{\mathrm{b}} f_{\mathrm{st,b}}} q_{\mathrm{b}}. \qquad [\Omega] \quad (7)$$

5. Coupling-current sub-networks

The innovative approach proposed here aims at reproducing with a limited number of equations the overall effect on the magnet behavior of local inter-filament and inter-strand coupling currents. The analysis of the electro-magnetic transient follows the equivalent magnetization model described in [7] and refers to the equivalent network model presented in [8].

The LEDET coupling model is composed of three sub-networks simulating the effect of inter-filament coupling currents in the two directions

Table 1: Electro-thermal analogy implemented in the LEDET model, for a generic block b. Symbols pertaining to the electrical domain refer to figure 5.

Thermal domain		Electrical domain	
T_{b}	[K]	U_{b}	[V]
T_{h}	[K]	U_{h}	[V]
T_{He}	[K]	U_{He}	[V]
$P_{\mathrm{if,b}}$	[W]	$I_{\mathrm{if,b}}$	[A]
$P_{\mathrm{is,b}}$	[W]	$I_{\mathrm{is,b}}$	[A]
$P_{\mathrm{ohm,b}}$	[W]	$I_{\mathrm{ohm,b}}$	[A]
$C_{\mathrm{b}}(T_{\mathrm{b}})$	[JK^{-1}]	$C_{\mathrm{th,b}}$	[F]
$\frac{1}{A_{\mathrm{b,h}}} \frac{s_{\mathrm{h}} k_{\mathrm{b}}(T_{\mathrm{b}}) + s_{\mathrm{b}} k_{\mathrm{h}}(T_{\mathrm{h}})}{k_{\mathrm{b}}(T_{\mathrm{b}}) k_{\mathrm{h}}(T_{\mathrm{h}})}$	[KW^{-1}]	$R_{\mathrm{b,h}}$	[Ω]
$\frac{1}{h_{\mathrm{He,b}}(T_{\mathrm{b}}, T_{\mathrm{He}}) A_{\mathrm{b,He}}}$	[KW^{-1}]	$R_{\mathrm{He,b}}$	[Ω]

perpendicular to the magnet transport current and of inter-strand coupling currents in the direction perpendicular to the cable broad face, respectively.

Each coupling sub-network is further subdivided into N_{CL} blocks, each modeling effects occurring in a certain volume of conductor. For the sake of simplicity, it is here assumed that each block cl of the coupling sub-network corresponds to one block b of the thermal sub-network presented in the previous section ($cl \equiv b$).

5.1. Equivalent IFCC loops

Consider the case of a strand, or wire, of circular cross-section and of radius r_{s} [m], whose superconducting filaments are homogeneously distributed along its diameter d_{s} [m]. This assumption is chosen for the sake of simplicity, but the results of this section can be easily extended to less general cases by modifying the value of the effective transverse resistivity of the strand stabilizer matrix, ρ_{eff} [Ωm], as explained in section 5.1.1 [1, 23, 24].

When the strand is subject to a magnetic-field change in a direction $\overrightarrow{e}_{\mathrm{x}'}$ perpendicular to the direction $\overrightarrow{e}_{\mathrm{z}'}$ of the transport current, a surface current-density arises along the circumference $r{=}r_{\mathrm{s}}$. Following [7, 9, 8, 4],

this surface current-density can be expressed as

$$\overrightarrow{K}_{\mathrm{if}} = -\left(\frac{l_{\mathrm{f}}}{2\pi}\right)^2 \frac{1}{\rho_{\mathrm{eff}}} \frac{dB_{\mathrm{t}}}{dt} \cos(\phi)\ \overrightarrow{e}_{\mathrm{z}'}, \qquad [\mathrm{Am}^{-1}] \quad (8)$$

where l_{f} [m] is the filament twist-pitch, dB_{t}/dt [Ts^{-1}] is the absolute value of the total magnetic field change, defined in equation 1, and $\phi{=}\pi/2{-}2\pi z/l_{\mathrm{f}}$ [rad].

The magnetic moment of a current distribution $\overrightarrow{J}$ is computed as $\overrightarrow{m}{=}\frac{1}{2}\int_{\mathscr{V}} \overrightarrow{r}{\times}\overrightarrow{J}\ dV$ [Am]. For extruded loops of surface currents $\overrightarrow{K}_{\mathrm{if}}$ on the boundary $\partial\mathscr{V}$ of $\mathscr{V}$ we define

$$\begin{aligned} \overrightarrow{m}' &= \lim_{\ell\longrightarrow\infty} \frac{1}{2\ell} \int_{\mathscr{V}} \overrightarrow{r} \times \overrightarrow{J}\ dV \\ &= \lim_{\ell\longrightarrow\infty} \frac{1}{2\ell} \int_{\partial\mathscr{V}} \overrightarrow{r} \times \overrightarrow{K}_{\mathrm{if}}\ da \qquad [\mathrm{A\ m}] \quad (9) \\ &= \int_{\partial\mathscr{A}} \overrightarrow{r} \times \overrightarrow{K}_{\mathrm{if}}\ ds, \end{aligned}$$

where the surface $\mathscr{A}$ is the cross-section of $\mathscr{V}$ in the extruded part and the factor two between the second and third lines is due to the omission of the path closure at $\pm\ell$. Hence, by combining equations 8 and 9, one obtains

$$\begin{aligned} \overrightarrow{m}'_{\mathrm{if}} &= \int_0^{2\pi} \overrightarrow{r} \times \overrightarrow{K}_{\mathrm{if}} r_{\mathrm{s}} d\phi \\ &= \overrightarrow{e}_{\mathrm{y}'} \int_0^{\pi/2} r_{\mathrm{s}} \cos(\phi) K_{\mathrm{if}} r_{\mathrm{s}} d\phi \\ &= -\overrightarrow{e}_{\mathrm{y}'} \int_0^{\pi/2} \left(\frac{l_{\mathrm{f}}}{2\pi}\right)^2 \frac{1}{\rho_{\mathrm{eff}}} \frac{dB_{\mathrm{t}}}{dt} {r_{\mathrm{s}}}^2 \cos^2(\phi) d\phi \qquad [\mathrm{Am}] \quad (10) \\ &= -\left(\frac{l_{\mathrm{f}}}{2\pi}\right)^2 \frac{1}{\rho_{\mathrm{eff}}} \frac{dB_{\mathrm{t}}}{dt} \pi {r_{\mathrm{s}}}^2 \overrightarrow{e}_{\mathrm{y}'}. \end{aligned}$$

The equivalent magnetization can be derived from $\overrightarrow{m}'_{\mathrm{if}} = \overrightarrow{M}_{\mathrm{if}} \pi {r_{\mathrm{s}}}^2$:

$$\overrightarrow{M}_{\mathrm{if}} = -\left(\frac{l_{\mathrm{f}}}{2\pi}\right)^2 \frac{1}{\rho_{\mathrm{eff}}} \frac{dB_{\mathrm{t}}}{dt} \overrightarrow{e}_{\mathrm{y}'}. \qquad [\mathrm{Am}^{-1}] \quad (11)$$

Note that $\overrightarrow{M}_{\mathrm{if}}$ is homogeneous in the strand within the layer of superconducting filaments ($r{<}r_{\mathrm{s}}{=}d_{\mathrm{s}}/2$), which in the present case corresponds to the entire strand volume.

By integrating $\overrightarrow{K}_{\mathrm{if}}$ along the circumference where the filaments are situated, the total current I_{if} [A] flowing at either side of the strand can be calculated:

$$I_{\mathrm{if}} = 2\int_0^{\pi/2} K_{\mathrm{if}} r_{\mathrm{s}} d\phi = \left(\frac{l_{\mathrm{f}}}{2\pi}\right)^2 \frac{1}{\rho_{\mathrm{eff}}} \frac{dB_{\mathrm{t}}}{dt} d_{\mathrm{s}}. \qquad [\mathrm{A}] \quad (12)$$

By combining equations 11 and 12, one obtains

$$\overrightarrow{M}_{\mathrm{if}} = \frac{\overrightarrow{I}_{\mathrm{if}}}{d_{\mathrm{s}}}, \qquad [\mathrm{Am}^{-1}] \quad (13)$$

where the vectorial $\overrightarrow{I}_{\mathrm{if}}$ is introduced as the pair of currents ($I_{\mathrm{if,x}}$, $I_{\mathrm{if,y}}$) in the x- and y- directed dipoles such that the above equation is fulfilled. Note the distinction between the directions ($\overrightarrow{e}_{\mathrm{x'}}$; $\overrightarrow{e}_{\mathrm{y'}}$) parallel and perpendicular to the applied magnetic-field change, respectively; and the directions (x; y) defined in an external orthogonal frame, arbitrarily chosen and common to all strands in the magnet.

The magnetic field induced in the strand by the magnetic-field change can be computed following [4], as

$$\begin{aligned} B_{\mathrm{if}} &= \int_0^{2\pi} \frac{\mu_0 K_{\mathrm{if}}}{2\pi r} \cos(\phi) r d\phi \\ &= -\int_0^{2\pi} \frac{\mu_0}{2\pi} \left(\frac{l_{\mathrm{f}}}{2\pi}\right)^2 \frac{1}{\rho_{\mathrm{eff}}} \frac{dB_{\mathrm{t}}}{dt} \cos^2(\phi) d\phi \\ &= -\frac{\mu_0}{2} \left(\frac{l_{\mathrm{f}}}{2\pi}\right)^2 \frac{1}{\rho_{\mathrm{eff}}} \frac{dB_{\mathrm{t}}}{dt} \\ &= -\frac{\mu_0}{2} \beta_{\mathrm{if}} \frac{dB_{\mathrm{t}}}{dt}, \end{aligned} \qquad [\mathrm{T}] \quad (14)$$

where $\beta_{\mathrm{if}} = \left(\frac{l_{\mathrm{f}}}{2\pi}\right)^2 \frac{1}{\rho_{\mathrm{eff}}}$ is introduced. By combining equations 11-14, one obtains

$$\overrightarrow{B}_{\mathrm{if}} = \frac{\mu_0}{2} \overrightarrow{M}_{\mathrm{if}} = \frac{\mu_0}{2d_{\mathrm{s}}} \overrightarrow{I}_{\mathrm{if}}. \qquad [\mathrm{T}] \quad (15)$$

Furthermore, with the IFCL time-constant often proposed in the literature [7, 8],

$$\tau_{\mathrm{if}} = \frac{\mu_0}{2} \left(\frac{l_{\mathrm{f}}}{2\pi}\right)^2 \frac{1}{\rho_{\mathrm{eff}}} = \frac{\mu_0}{2} \beta_{\mathrm{if}}, \qquad [\mathrm{s}] \quad (16)$$

and defining a tensorial time constant τ_{if},

$$\begin{cases} \tau_{\mathrm{if,x}} = \dfrac{\mu_0}{2}\dfrac{1}{\rho_{\mathrm{eff,x}}}\left(\dfrac{l_{\mathrm{f}}}{2\pi}\right)^2 = \dfrac{\mu_0}{2}\beta_{\mathrm{if,x}} \\ \tau_{\mathrm{if,y}} = \dfrac{\mu_0}{2}\dfrac{1}{\rho_{\mathrm{eff,y}}}\left(\dfrac{l_{\mathrm{f}}}{2\pi}\right)^2 = \dfrac{\mu_0}{2}\beta_{\mathrm{if,y}}, \end{cases} \quad [\mathrm{s}] \quad (17)$$

it follows that the total magnetic-field change is

$$\frac{d\overrightarrow{B}_{\mathrm{t}}}{dt} = -\tau_{\mathrm{if}}^{-1}\overrightarrow{B}_{\mathrm{if}} = -\frac{\mu_0}{2}\tau_{\mathrm{if}}^{-1}\overrightarrow{M}_{\mathrm{if}} = -\beta_{\mathrm{if}}^{-1}\overrightarrow{M}_{\mathrm{if}} = -\beta_{\mathrm{if}}^{-1}\frac{\overrightarrow{I}_{\mathrm{if}}}{d_{\mathrm{s}}}. \quad [\mathrm{Ts}^{-1}] \quad (18)$$

The tensorial effective transverse resistivity $\rho_{\mathrm{eff}}=(\rho_{\mathrm{eff,x}}, \rho_{\mathrm{eff,y}})$ occurring in β_{if} depends on the absolute magnetic field in the copper matrix due to magneto-resistivity effects, as shown in section 5.1.1. Note that in the most general case the effective resistivities in the x and y directions may differ $(\rho_{\mathrm{eff,x}}\neq\rho_{\mathrm{eff,y}})$.

Let $\mathscr{A}_{\mathrm{s}}$ be the reference strand surface delimited by the outer layer of superconducting filaments; and let $|\mathscr{A}_{\mathrm{s}}|=a_{\mathrm{s}}=\pi {r_{\mathrm{s}}}^2$ be its metric measure. The loss per unit length of conductor generated by the inter-filament coupling currents are computed using

$$\begin{aligned} P'_{\mathrm{if}} &= -\int_{\mathscr{A}_{\mathrm{s}}} \overrightarrow{M}_{\mathrm{if}} \cdot \frac{d\overrightarrow{B}_{\mathrm{t}}}{dt} da \\ &= -\overrightarrow{M}_{\mathrm{if}} \cdot \frac{d\overrightarrow{B}_{\mathrm{t}}}{dt} a_{\mathrm{s}} \\ &= \beta_{\mathrm{if}} \left(\frac{dB_{\mathrm{t}}}{dt}\right)^2 a_{\mathrm{s}}. \end{aligned} \quad [\mathrm{Wm}^{-1}] \quad (19)$$

Note that dividing this equation by the strand surface a_{s} yields an expression of the inter-filament coupling loss identical to the classical formulation [7, 8]. Furthermore, by rearranging the equation it is possible to obtain an explicit relation between IFCL and IFCC,

$$\begin{aligned} P'_{\mathrm{if}} &= P'_{\mathrm{if,x}} + P'_{\mathrm{if,y}} \\ &= \frac{a_{\mathrm{s}}}{{d_{\mathrm{s}}}^2}\left(\frac{I^2_{\mathrm{if,x}}}{\beta_{\mathrm{if,x}}} + \frac{I^2_{\mathrm{if,y}}}{\beta_{\mathrm{if,y}}}\right) \\ &= R'_{\mathrm{if,x}} I^2_{\mathrm{if,x}} + R'_{\mathrm{if,y}} I^2_{\mathrm{if,y}} \\ &= \vec{I}^T_{\mathrm{if}} R'_{\mathrm{if}} \vec{I}_{\mathrm{if}}, \end{aligned} \quad [\mathrm{Wm}^{-1}] \quad (20)$$

where a tensorial resistance per unit length R'_{if} is defined following

$$\begin{cases} R'_{\mathrm{if,x}} = \dfrac{a_{\mathrm{s}}}{{d_{\mathrm{s}}}^2}\dfrac{1}{\beta_{\mathrm{if,x}}} = \dfrac{\pi}{4}\dfrac{1}{\beta_{\mathrm{if,x}}} \\ R'_{\mathrm{if,y}} = \dfrac{a_{\mathrm{s}}}{{d_{\mathrm{s}}}^2}\dfrac{1}{\beta_{\mathrm{if,y}}} = \dfrac{\pi}{4}\dfrac{1}{\beta_{\mathrm{if,y}}}. \end{cases} \qquad [\Omega \mathrm{m}^{-1}] \quad (21)$$

These defined parameters can be regarded as the resistances of equivalent inter-filament dissipative loops. The self-inductance per unit length of conductor of such equivalent loops can be computed with the "winding density" $\overrightarrow{k}_{\mathrm{if}} = \overrightarrow{K}_{\mathrm{if}}/I_{\mathrm{if}}$ [m^{-1}], from

$$\begin{aligned} L'_{\mathrm{if}} = L'_{\mathrm{if,x}} = L'_{\mathrm{if,y}} &= \frac{1}{I_{\mathrm{if}}} \int_{\partial \mathscr{A}_{\mathrm{s}}} \overrightarrow{k}_{\mathrm{if}} \cdot \overrightarrow{A}_{\mathrm{if}} ds \\ &= \frac{\mu_0 \pi}{8} = \frac{\mu_0 a_{\mathrm{s}}}{2{d_{\mathrm{s}}}^2}, \end{aligned} \qquad [\mathrm{Hm}^{-1}] \quad (22)$$

where $\overrightarrow{A}_{\mathrm{if}} = \frac{d_{\mathrm{s}}}{2} B_{\mathrm{if}} \cos(\phi) \overrightarrow{e}'_{\mathrm{z}}$. Consistently, the resulting RL constant of the introduced equivalent IFCC loops equals the IFCL time-constant introduced in equation 16,

$$\tau_{\mathrm{if}} = \frac{L'_{\mathrm{if}}}{R'_{\mathrm{if}}} = \frac{\mu_0}{2}\beta_{\mathrm{if}}. \qquad [\mathrm{s}] \quad (23)$$

Moreover, the local IFCC influence the behavior of the elements composing the electrical sub-network presented in section 3. A relation describing this interaction can be derived from the equation of local magnetic-field change. The total magnetic-field change is the result of the applied magnetic-field change $d\overrightarrow{B}_{\mathrm{a}}/dt$ generated by a change in the local currents, and the already defined $d\overrightarrow{B}_{\mathrm{if}}/dt$ which opposes to the change [8]:

$$\frac{d\overrightarrow{B}_{\mathrm{t}}}{dt} = \frac{d\overrightarrow{B}_{\mathrm{a}}}{dt} + \frac{d\overrightarrow{B}_{\mathrm{if}}}{dt}. \qquad [\mathrm{Ts}^{-1}] \quad (24)$$

The applied magnetic-field change can be expressed as the superposition of the field change generated by the change in the local currents of the N_{E} elements in the electrical sub-network,

$$\begin{cases} \dfrac{dB_{\mathrm{a,x}}}{dt} = \displaystyle\sum_{e=1}^{N_{\mathrm{E}}} f_{\mathrm{e,x}} \frac{dI_{\mathrm{e}}}{dt} \\ \dfrac{dB_{\mathrm{a,y}}}{dt} = \displaystyle\sum_{e=1}^{N_{\mathrm{E}}} f_{\mathrm{e,y}} \frac{dI_{\mathrm{e}}}{dt}, \end{cases} \qquad [\mathrm{Ts}^{-1}] \quad (25)$$

where the parameters $\overrightarrow{f}_{\mathrm{e}}=(f_{\mathrm{e,x}}, f_{\mathrm{e,y}})$ [TA^{-1}] can be calculated by means of dedicated software, such as ROXIE [25] or SOLENO [26]. In first approximation, they are purely geometric.

By substituting equations 18, 25, and 15 into 24; and multiplying by $a_{\mathrm{s}}/d_{\mathrm{s}}$, an equation for induced voltages, i.e. time-derivatives of linked magnetic fluxes, per unit length is derived:

$$-\frac{a_{\mathrm{s}}}{{d_{\mathrm{s}}}^2}\frac{1}{\beta_{\mathrm{if}}}\overrightarrow{I}_{\mathrm{if}} = \frac{a_{\mathrm{s}}}{d_{\mathrm{s}}}\sum_{e=1}^{N_{\mathrm{E}}}\overrightarrow{f}_{\mathrm{e}}\frac{dI_{\mathrm{e}}}{dt} + \frac{\mu_0 a_{\mathrm{s}}}{2{d_{\mathrm{s}}}^2}\frac{d\overrightarrow{I}_{\mathrm{if}}}{dt}, \qquad [\mathrm{Vm}^{-1}] \quad (26)$$

where the parameters R'_{if} and L'_{if} introduced with equations 21 and 22 can be identified, together with tensorial mutual inductances per unit length $M'_{\mathrm{if,e}}$:

$$\begin{cases} M'_{\mathrm{if,e,x}} = \dfrac{a_{\mathrm{s}}}{d_{\mathrm{s}}}f_{\mathrm{e,x}} = \dfrac{\pi d_{\mathrm{s}}}{4}f_{\mathrm{e,x}} & \text{for } e = 1...N_{\mathrm{E}} \\ M'_{\mathrm{if,e,y}} = \dfrac{a_{\mathrm{s}}}{d_{\mathrm{s}}}f_{\mathrm{e,y}} = \dfrac{\pi d_{\mathrm{s}}}{4}f_{\mathrm{e,y}} & \text{for } e = 1...N_{\mathrm{E}}. \end{cases} \qquad [\mathrm{Hm}^{-1}] \quad (27)$$

Thus, equation 24 can be rewritten as

$$\begin{cases} -R'_{\mathrm{if,x}}I_{\mathrm{if,x}} = \displaystyle\sum_{e=1}^{N_{\mathrm{E}}} M'_{\mathrm{if,e,x}}\frac{I_{\mathrm{e}}}{dt} + L'_{\mathrm{if,x}}\frac{I_{\mathrm{if,x}}}{dt} \\ -R'_{\mathrm{if,y}}I_{\mathrm{if,y}} = \displaystyle\sum_{e=1}^{N_{\mathrm{E}}} M'_{\mathrm{if,e,y}}\frac{I_{\mathrm{e}}}{dt} + L'_{\mathrm{if,y}}\frac{I_{\mathrm{if,y}}}{dt} \end{cases} \qquad [\mathrm{Vm}^{-1}] \quad (28)$$

This set of equations describes the complex interaction between local IFCC and changes in the currents flowing in the main electrical circuit.

Finally, the overall effect on the system dynamics of the local IFCC in a volume of conductor can be calculated by superposition of effects. Let us consider the case of a model block b, composed of $N_{\mathrm{c,b}}$ conductors with length l_{b} [m], as defined in equation 3; each conductor being composed of $N_{\mathrm{s,b}}$ superconducting strands. The volume of its strands is $V_{\mathrm{s,b}}=N_{\mathrm{c,b}}N_{\mathrm{s,b}}\pi\frac{{d_{\mathrm{s,b}}}^2}{4}l_{\mathrm{b}}$ [m^3]. By multiplying the equations of system 28 by $N_{\mathrm{c,b}}N_{\mathrm{s,b}}l_{\mathrm{b}}$, one obtains

$$\begin{cases} -R_{\mathrm{if,b,x}}I_{\mathrm{if,b,x}} = \displaystyle\sum_{e=1}^{N_{\mathrm{E}}} M_{\mathrm{if,b,e,x}}\frac{I_{\mathrm{e}}}{dt} + L_{\mathrm{if,b,x}}\frac{I_{\mathrm{if,b,x}}}{dt} \\ -R_{\mathrm{if,b,y}}I_{\mathrm{if,b,y}} = \displaystyle\sum_{e=1}^{N_{\mathrm{E}}} M_{\mathrm{if,b,e,y}}\frac{I_{\mathrm{e}}}{dt} + L_{\mathrm{if,b,y}}\frac{I_{\mathrm{if,b,y}}}{dt}, \end{cases} \qquad [\mathrm{V}] \quad (29)$$

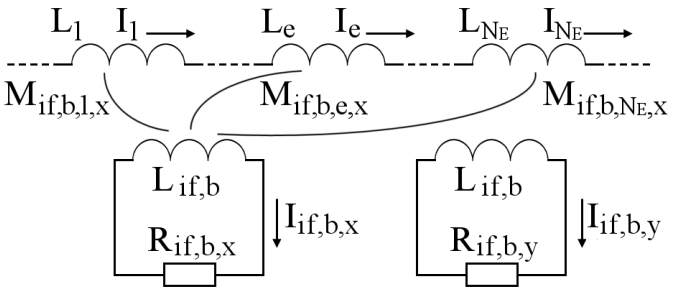

Figure 6: Equivalent LEDET sub-network modeling the inter-filament coupling currents in block b (mutual inductances $M_{\mathrm{if,b,1,y}}$, $M_{\mathrm{if,b,e,y}}$, and $M_{\mathrm{if,b,N_E,y}}$ are not shown).

where the tensorial equivalent resistance $R_{\mathrm{if,b}}$, self-inductance $L_{\mathrm{if,b}}$, and mutual inductances $M_{\mathrm{if,b,e}}$ of the IFCC loop representing the dynamic behavior of block b are defined as:

$$\begin{cases} R_{\mathrm{if,b,x}} = \dfrac{V_{\mathrm{s,b}}}{{d_{\mathrm{s,b}}}^2}\dfrac{1}{\beta_{\mathrm{if,b,x}}} = \dfrac{\pi}{4}N_{\mathrm{c,b}}N_{\mathrm{s,b}}l_{\mathrm{b}}\dfrac{1}{\beta_{\mathrm{if,b,x}}} & [\Omega] \\ R_{\mathrm{if,b,y}} = \dfrac{V_{\mathrm{s,b}}}{{d_{\mathrm{s,b}}}^2}\dfrac{1}{\beta_{\mathrm{if,b,y}}} = \dfrac{\pi}{4}N_{\mathrm{c,b}}N_{\mathrm{s,b}}l_{\mathrm{b}}\dfrac{1}{\beta_{\mathrm{if,b,y}}} & [\Omega] \\ L_{\mathrm{if,b}} = L_{\mathrm{if,b,x}} = L_{\mathrm{if,b,y}} = \dfrac{\mu_0}{2}\dfrac{V_{\mathrm{s,b}}}{{d_{\mathrm{s,b}}}^2} = \dfrac{\mu_0\pi}{8}N_{\mathrm{c,b}}N_{\mathrm{s,b}}l_{\mathrm{b}} & [\mathrm{H}] \\ M_{\mathrm{if,b,e,x}} = \dfrac{V_{\mathrm{s,b}}}{d_{\mathrm{s,b}}}f_{\mathrm{b,e,x}} = \dfrac{\pi}{4}N_{\mathrm{c,b}}N_{\mathrm{s,b}}d_{\mathrm{s,b}}l_{\mathrm{b}}f_{\mathrm{b,e,x}} \quad \text{for } e = 1...N_{\mathrm{E}} & [\mathrm{H}] \\ M_{\mathrm{if,b,e,y}} = \dfrac{V_{\mathrm{s,b}}}{d_{\mathrm{s,b}}}f_{\mathrm{b,e,y}} = \dfrac{\pi}{4}N_{\mathrm{c,b}}N_{\mathrm{s,b}}d_{\mathrm{s,b}}l_{\mathrm{b}}f_{\mathrm{b,e,y}} \quad \text{for } e = 1...N_{\mathrm{E}}. & [\mathrm{H}] \end{cases} \tag{30}$$

The behavior of the set of equations 29 can be modeled with an equivalent lumped-element circuit composed of two closed loops of a resistor and a self-inductance mutually coupled to the N_{E} self-inductances L_{e} present in the electrical sub-network. Figure 6 shows a schematic representation of such a circuit. In order to model the IFCC effects in the x and y direction in the N_{B} blocks of the coupling sub-network, $2N_{\mathrm{B}}$ similar equivalent loops are implemented.

In addition to the coupling between local IFCC and system currents, the introduced model provides a calculation of the inter-filament coupling loss in each block. In fact, the ohmic loss dissipated in each equivalent resistor $R_{\mathrm{if,b}}$

corresponds to the IFCL in the matrix of the strands of block b:

$$\begin{aligned} P_{\mathrm{if,b}} &= P_{\mathrm{if,b,x}} + P_{\mathrm{if,b,y}} \\ &= \vec{I}^{\mathrm{T}}_{\mathrm{if,b}} R'_{\mathrm{if,b}} \vec{I}_{\mathrm{if,b}} = R_{\mathrm{if,b,x}} I^2_{\mathrm{if,b,x}} + R_{\mathrm{if,b,y}} I^2_{\mathrm{if,b,y}}. \end{aligned} \qquad [\mathrm{W}] \quad (31)$$

The loss calculated with this equation is used to solve the thermal balance in block b presented in equation 2.

Most of the parameters present in the definitions 30 are geometrical or physical quantities. However, the introduced model includes an unknown parameter, namely the effective transverse resistivity of the strand matrix, which is inversely proportional to $\beta_{\mathrm{if,b}}$. The value of the effective transverse resistivity for a certain strand, or wire, can be deduced by measuring the transitory loss occurring in a single wire of the same type. Alternatively, its value can be estimated with the procedure explained in the next section.

5.1.1. Effective transverse resistivity

The effective resistivity in a direction x perpendicular to the transport current is calculated as

$$\rho_{\mathrm{eff,x}} = \rho_{\mathrm{m}} f_{\mathrm{eff,x}} = (c_0 + c_1 B_{\mathrm{t}})\, f_{\mathrm{eff,x}}, \qquad [\Omega\mathrm{m}] \quad (32)$$

where ρ_{m} [Ωm] is the electrical resistivity of the matrix material, c_0 [Ωm] and c_1 [$\Omega\mathrm{mT}^{-1}$] are parameters depending on the residual resistivity ratio (RRR) and magneto-resistivity of the material used as matrix, and usually known from the literature [27], and $f_{\mathrm{eff,x}}$ is a parameter depending on the fraction of superconductor in the matrix, on the interface resistance between the filaments and the matrix, and on the position of the filaments over the strand cross-section [28, 29, 30]. In the most general case the effective resistivities in the x and y directions perpendicular to the transport current may differ ($\rho_{\mathrm{eff,x}} \neq \rho_{\mathrm{eff,y}}$); hence, the time constants of the coupling currents in the two directions can be different as well ($\tau_{\mathrm{if,x}} \neq \tau_{\mathrm{if,y}}$).

In the case of a round strand with a fraction of superconductor f_{sc}, whose superconducting filaments are uniformly distributed in a matrix of a single material, it is found that the value of the effective parameter $f_{\mathrm{eff}} = f_{\mathrm{eff,x}} = f_{\mathrm{eff,y}}$ is

$$f_{\mathrm{eff}} = \frac{1 - f_{\mathrm{sc}}}{1 + f_{\mathrm{sc}}}, \qquad \text{or} \qquad f_{\mathrm{eff}} = \frac{1 + f_{\mathrm{sc}}}{1 - f_{\mathrm{sc}}}, \quad (33)$$

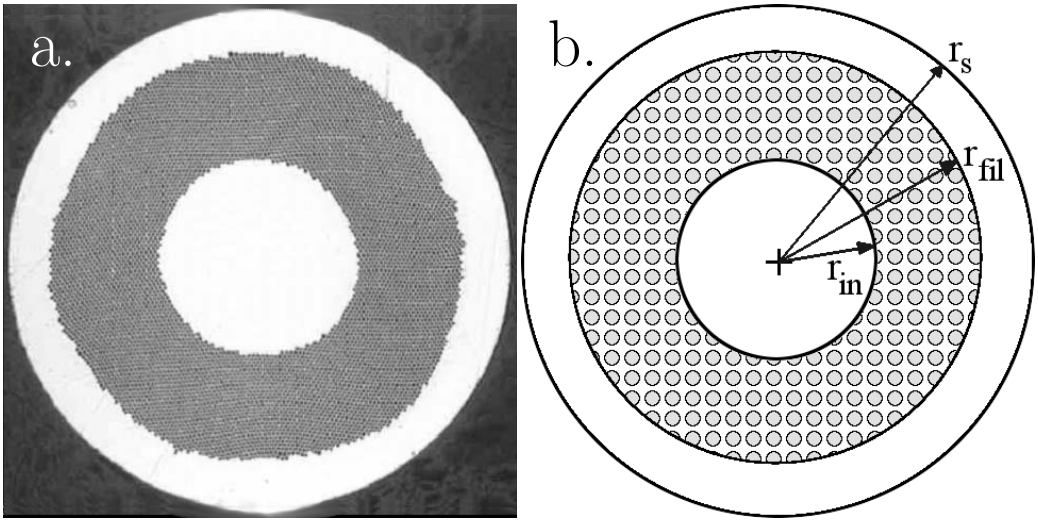

Figure 7: Cross-section of the strand used in the cable of the outer layer of the LHC main dipole magnets [31]. a. Photography. b. Schematic representation.

in the case the superconducting filaments do or do not contribute to the transverse conduction, respectively [28, 29, 30, 8]. The former case occurs for small interface resistance between the filaments and the matrix; whereas the latter occurs if the interface resistance is large. Any value in between these two extremes may be reached if the interface resistance has an intermediate value.

Strands used in nowadays superconducting magnets often include a bundle of superconducting filaments embedded in a matrix, plus an inner core and/or an outer shell of stabilizer. As an example, consider the strand shown in figure 7a, used in the cable of the outer layer of the LHC main dipole magnets [31]. When such a strand is exposed to a magnetic-field change, different inter-filament coupling loss is generated in the volume of the inner stabilizer core ($0<r<r_{\mathrm{in}}$, see figure 7b), in the annular ring where the superconducting filaments are located ($r_{\mathrm{in}}<r<r_{\mathrm{fil}}$), and in the outer stabilizer shell ($r_{\mathrm{fil}}<r<r_{\mathrm{s}}$). Following the treatise presented in [23, 24], these three loss contributions, per unit volume of strand, are

$$P'''_{\mathrm{in}} = \left(\frac{l_{\mathrm{f}}}{2\pi}\right)^2 \frac{1}{\rho_{\mathrm{m}}} \frac{r_{\mathrm{in}}^2}{r_{\mathrm{s}}^2} \left(\frac{dB_{\mathrm{t}}}{dt}\right)^2, \qquad [\mathrm{Wm}^{-3}] \quad (34)$$

$$P'''_{\mathrm{fil}} = \left(\frac{l_{\mathrm{f}}}{2\pi}\right)^2 \frac{1}{\rho_{\mathrm{eff,fil}}} \left(\frac{r_{\mathrm{fil}}^2 - r_{\mathrm{in}}^2}{r_{\mathrm{s}}^2}\right) \left(\frac{dB_{\mathrm{t}}}{dt}\right)^2, \quad [\mathrm{Wm}^{-3}] \quad (35)$$

$$P'''_{\text{out}} = \left(\frac{l_\text{f}}{2\pi}\right)^2 \frac{1}{\rho_\text{m}} \left(\frac{r_\text{s}^2 - r_\text{fil}^2}{r_\text{s}^2 + r_\text{fil}^2}\right) \left(\frac{dB_\text{t}}{dt}\right)^2, \qquad [\text{Wm}^{-3}] \quad (36)$$

where $\rho_{\text{eff,fil}}$ [Ωm] is the effective transverse resistivity in the region occupied by the bundle of filaments. Its value is comprised in the range between the two extremes defined in equation 33.

Thus, equation 19 can still be used for the calculation of the power per unit volume of strand generated by inter-filament coupling loss, if the effective transverse resistivity is calculated with equation 32 and the value of f_eff is corrected as follows:

$$f_\text{eff} = \frac{\rho_\text{eff}}{\rho_\text{m}} = \left[\frac{r_\text{in}^2}{r_\text{s}^2} + \frac{1}{\rho_{\text{eff,fil}}} \left(\frac{r_\text{fil}^2 - r_\text{in}^2}{r_\text{s}^2}\right) + \left(\frac{r_\text{s}^2 - r_\text{fil}^2}{r_\text{s}^2 + r_\text{fil}^2}\right)\right]^{-1}. \quad (37)$$

5.2. Equivalent ISCC loops

As mentioned in section 2.2, if a conductor is composed of multiple superconducting strands, inter-strand coupling currents develop. The following treatise only considers ISCC through cross-contact resistance and due to a magnetic-field change perpendicular to the cable broad face. These currents typically generate the largest fraction of the ISCL in the cable [8].

The model adopts an approach analogous to that applied in section 5.1 for the inter-filament coupling currents. The mutual coupling between local ISCC in a cable and the change of the currents in the main electrical circuit is described with a limited set of equations and modeled with an equivalent sub-network composed of equivalent ISCC loops.

Consider the case of a flat Rutherford cable, with large aspect ratio α_c=w/h, with w [m] and h [m] the broad and narrow cable dimension, respectively. Its surface $\mathscr{A}_\text{c}$ has metric measure $|\mathscr{A}_\text{c}|$=a_c=wh [m^2]. A magnetic-field change in the direction $\overrightarrow{e}_\perp$ perpendicular to the cable broad face induces ISCC through the contact resistance between two crossing strands, R_c [Ω]. The equivalent magnetization $\overrightarrow{M}_\text{is}$ [Am^{-1}] generated by these ISCC can be represented as the effect of an equivalent surface current flowing at the surface of the two sides of the cable,

$$\overrightarrow{K}_\text{is} = \overrightarrow{M}_\text{is} \times \overrightarrow{e}_\parallel = M_\text{is} \overrightarrow{e}_{z'}, \qquad [\text{Am}^{-1}] \quad (38)$$

where $\overrightarrow{e}_\parallel$ and $\overrightarrow{e}_{z'}$ are the directions parallel to the cable broad face and to the transport current, respectively. Thus, the equivalent ISCC flowing at either side of the cable is

$$\overrightarrow{I}_\text{is} = \overrightarrow{K}_\text{is} h = M_\text{is} h \overrightarrow{e}_{z'}. \qquad [\text{A}] \quad (39)$$

The inter-strand coupling loss per unit length of conductor can be calculated as

$$P'_{\mathrm{is}} = -\int_{\mathscr{A}_{\mathrm{c}}} \overrightarrow{M}_{\mathrm{is}} \cdot \frac{d\overrightarrow{B}_{\mathrm{t},\perp}}{dt} da, \qquad [\mathrm{Wm}^{-1}] \quad (40)$$

analogous to equation 19, where $dB_{\mathrm{t},\perp}/dt$ [Ts^{-1}] is the total magnetic field change in the direction $\overrightarrow{e}_{\perp}$. Note that $\overrightarrow{M}_{\mathrm{is}}$ and $\overrightarrow{B}_{\mathrm{t},\perp}$ are not homogeneous along the direction $\overrightarrow{e}_{\parallel}$. However, for various applications the assumption of homogeneous equivalent magnetization in the cable cross-section is acceptable. For example, in [7] it is proposed

$$\begin{aligned} \overrightarrow{M}'_{\mathrm{is}} &= -\frac{1}{120}\frac{l_{\mathrm{s}}}{R_{\mathrm{c}}} N_{\mathrm{s}} \left(N_{\mathrm{s}} - 1\right) \frac{w}{h} \frac{dB_{\mathrm{t},\perp}}{dt} \overrightarrow{e}_{\perp} \\ &= -\beta_{\mathrm{is}} \frac{dB_{\mathrm{t},\perp}}{dt} \overrightarrow{e}_{\perp}, \end{aligned} \qquad [\mathrm{Am}^{-1}] \quad (41)$$

with l_{s} [m] the strand twist-pitch and N_{s} the number of strands in the cable. Under this assumption, equations 39-41 can be combined leading to

$$\begin{aligned} P'_{\mathrm{is}} &= \beta_{\mathrm{is}} \left(\frac{dB_{\mathrm{t},\perp}}{dt}\right)^2 a_{\mathrm{c}} \\ &= \frac{w}{h}\frac{1}{\beta_{\mathrm{is}}} I_{\mathrm{is}}^2 \\ &= R'_{\mathrm{is}} I_{\mathrm{is}}^2, \end{aligned} \qquad [\mathrm{Wm}^{-1}] \quad (42)$$

where the equivalent resistance per unit length of the equivalent ISCC loop is identified:

$$R'_{\mathrm{is}} = \frac{w}{h}\frac{1}{\beta_{\mathrm{is}}} = \frac{\alpha_{\mathrm{c}}}{\beta_{\mathrm{is}}}. \qquad [\Omega\mathrm{m}^{-1}] \quad (43)$$

Note the analogy with the definition of R'_{if} in equation 21. The self-inductance of the ISCC loop can be evaluated by considering the effect of a surface current flowing at the two sides of the cable and generating a magnetic field $\overrightarrow{B}_{\mathrm{is}}$ [T], not homogeneous along the direction $\overrightarrow{e}_{\parallel}$. The self-inductance per unit length of this system can be approximated as

$$\begin{aligned} L'_{\mathrm{is,c}} &= \frac{1}{I_{\mathrm{is}}^2} \int_{\mathscr{A}_{\mathrm{c}}} \overrightarrow{M}_{\mathrm{is}} \cdot \overrightarrow{B}_{\mathrm{is}} da \\ &\sim \frac{\mu_0}{\pi} \left[\ln\left(\frac{w}{h}\right) + \frac{3}{2}\right], \end{aligned} \qquad [\mathrm{Hm}^{-1}] \quad (44)$$

where the approximated formula for the self-inductance per unit length of a pair of infinitely thin strip conductors presented in [32] is used. Thus, the resulting time-constant of the equivalent ISCC loop is

$$\tau_{\mathrm{is,c}} = \frac{L'_{\mathrm{is,c}}}{R'_{\mathrm{is}}} = \frac{\mu_0}{\pi}\left[\ln\left(\frac{w}{h}\right) + \frac{3}{2}\right]\frac{h}{w}\beta_{\mathrm{is}} = \frac{\mu_0}{\pi}\left[\ln\left(\alpha_{\mathrm{c}}\right) + \frac{3}{2}\right]\frac{\beta_{\mathrm{is}}}{\alpha_{\mathrm{c}}}. \quad [\mathrm{s}] \quad (45)$$

The values of $\tau_{\mathrm{is,c}}$ calculated with this model prove to be a good approximation of the more precise ISCC time-constant obtained with a more detailed equivalent-network model [8]. As an example, the model proposed in [8] predicts an ISCC time-constant of

$$\tau_{\mathrm{is,c,net}} = c_{\mathrm{s}} l_{\mathrm{s}} \frac{N_{\mathrm{s}}^2 - 4N_{\mathrm{s}}}{R_{\mathrm{c}}}, \quad [\mathrm{s}] \quad (46)$$

valid for Rutherford cables with $8 \leq N_{\mathrm{s}} \leq 40$, where c_{s} is a constant with a value between 1.6 and 1.7 10^{-8} $\Omega\mathrm{sm}^{-1}$ [8]. The comparison between the ISCC time-constant calculated with equation 45 and the time constant resulting from equation 46, for l_{s}=100 mm, R_{c}=100 $\mu\Omega$, and N_{s} in the range 8 to 40, is shown in figure 8.

If N_{c} cables are stacked, the total height of the stack $N_{\mathrm{c}}h$ is comparable or larger than w and the approximation of infinitely thin strips is not acceptable. Hence, equation 44 does not hold and the resulting ISCC time-constant is not correct. When a sufficient number of cables are stacked the approximation of induced magnetic field homogeneous in the surface $\mathscr{A}_{\mathrm{c}}$ and parallel to the magnetization lines is satisfactory:

$$\overrightarrow{B}_{\mathrm{is}} \sim \mu_0 \overrightarrow{M}_{\mathrm{is}} = \mu_0 \frac{\overrightarrow{I}_{\mathrm{is}}}{h}. \quad [\mathrm{T}] \quad (47)$$

Thus, the equivalent self-inductance of an ISCC loop modeling a cable which is part of a stack can be approximated as

$$\begin{aligned} L'_{\mathrm{is,st}} &= \frac{1}{I_{\mathrm{is}}^2}\int_{\mathscr{A}_{\mathrm{c}}} \overrightarrow{M}_{\mathrm{is}} \cdot \overrightarrow{B}_{\mathrm{is}}\, da \\ &\sim \mu_0 \left(\frac{M_{\mathrm{is}}}{I_{\mathrm{is}}}\right)^2 a_{\mathrm{c}} \qquad [\mathrm{Hm}^{-1}] \quad (48) \\ &= \mu_0 \frac{w}{h} = \mu_0 \alpha_{\mathrm{c}}, \end{aligned}$$

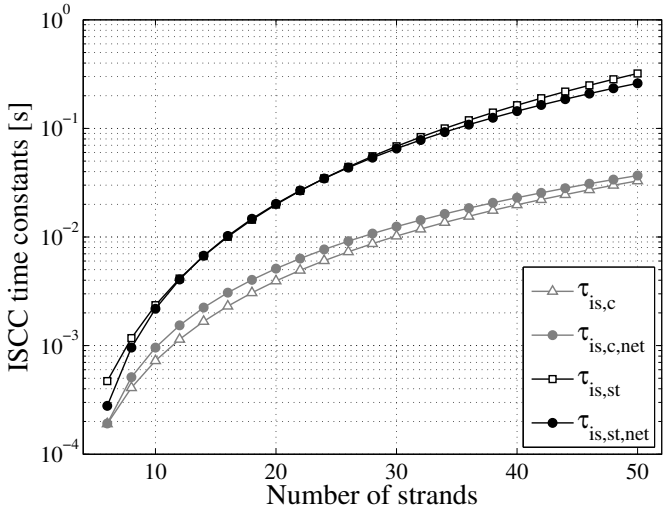

Figure 8: Comparison between the ISCC time-constant calculated using equation 45; or following the homogeneous-magnetization model presented in [7], see 49; or using the formulae derived in [8] with a complete network model for a single cable and for a stack of cables, see 46 and 50, respectively.

equivalent to the self-inductance of two parallel sheets carrying current when they are very close [33]. Note the similarity with L'_{if} introduced in equation 22. Thus, the resulting time constant of the equivalent ISCC loop for a cable in a stack is

$$\tau_{\mathrm{is,st}} = \frac{L'_{\mathrm{is,st}}}{R'_{\mathrm{is}}} = \mu_0 \beta_{\mathrm{is}}, \qquad [\mathrm{s}] \quad (49)$$

analogous to τ_{if} in equation 23. The more detailed equivalent-network model proposed in [8] predicts an overall ISCC time-constant for a stack of cables of

$$\tau_{\mathrm{is,st,net}} = \frac{\alpha_{\mathrm{c}} N_{\mathrm{c}}}{\alpha_{\mathrm{c}} + c_{\mathrm{st}} \left(N_{\mathrm{c}} - 1\right)} \tau_{\mathrm{is,c,net}}, \qquad [\mathrm{s}] \quad (50)$$

valid for $8 \leq N_{\mathrm{s}} \leq 40$, where c_{st} is a constant which depends slightly on the number of strands in the cable, increasing from about 1.00 for N_{s}=8 to 1.15 for N_{s}=40. An example calculation of the ISCC time-constant for a stack of cables calculated with equation 49, as compared to the time constant resulting from the detailed model [8], see equation 50, for N_{c}=15, α_{c}=N_{s}/4,

c_{st}=1, and N_{s} in the range 8 to 40, is shown in figure 8. The two calculations show very little difference across the entire range of N_{s}.

In conclusion, the time constant of an equivalent ISCC loop resulting from the proposed model with $L'_{\mathrm{is,c}}$ is a good approximation of the time constant for a single cable; and $L'_{\mathrm{is,st}}$ is a good approximation of the time constant for a cable which is part of a stack.

Furthermore, it is of high interest to model the mutual coupling between the local ISCC loops and the current-changes in the N_{E} self-inductances L_{e} present in the electrical sub-network defined in section 3. The local balance equation of the magnetic field change reads

$$\frac{dB_{\mathrm{t},\perp}}{dt} = \frac{dB_{\mathrm{a},\perp}}{dt} + \frac{dB_{\mathrm{is}}}{dt}, \qquad [\mathrm{Ts}^{-1}] \quad (51)$$

where the applied magnetic-field change $dB_{\mathrm{a},\perp}/dt$ [Ts^{-1}] can be expressed as the superposition of the magnetic-field change in the direction $\overrightarrow{e}_{\perp}$ generated by variations in the transport currents flowing in the electrical sub-network,

$$\frac{dB_{\mathrm{a},\perp}}{dt} = \sum_{e=1}^{N_{\mathrm{E}}} f_{\mathrm{e},\perp} \frac{dI_{\mathrm{e}}}{dt}, \qquad [\mathrm{Ts}^{-1}] \quad (52)$$

where the parameters $f_{\mathrm{e},\perp}$ [TA^{-1}] can be calculated by means of dedicated software, such as ROXIE [25] or SOLENO [26]. In first approximation, they are purely geometric. The assumption of homogeneous magnetic-field change in the cable cross-section, substituting equations 39, 41, 47, and 52 into 51 and multiplying by w, yields:

$$-\frac{w}{h}\frac{1}{\beta_{\mathrm{is}}}\overrightarrow{I}_{\mathrm{is}} = w\sum_{e=1}^{N_{\mathrm{E}}} \overrightarrow{f}_{\mathrm{e},\perp}\frac{dI_{\mathrm{e}}}{dt} + \mu_0\frac{w}{h}\frac{d\overrightarrow{I}_{\mathrm{is}}}{dt}, \qquad [\mathrm{Vm}^{-1}] \quad (53)$$

where the parameters R'_{is} and $L'_{\mathrm{is,st}}$ introduced with equations 43 and 48 can be identified, together with N_{E} mutual inductances per unit length:

$$M'_{\mathrm{is,e},\perp} = w f_{\mathrm{e},\perp}, \qquad \text{for } e = 1...N_{\mathrm{E}}, \qquad [\mathrm{Hm}^{-1}] \quad (54)$$

analogous to $M_{\mathrm{if,e}}$ defined in equation 27. Thus, equation 51 can be rewritten as

$$-R'_{\mathrm{is}}I_{\mathrm{is}} = \sum_{e=1}^{N_{\mathrm{E}}} M'_{\mathrm{is,e},\perp}\frac{dI_{\mathrm{e}}}{dt} + L'_{\mathrm{is,st}}\frac{dI_{\mathrm{is}}}{dt}. \qquad [\mathrm{Vm}^{-1}] \quad (55)$$

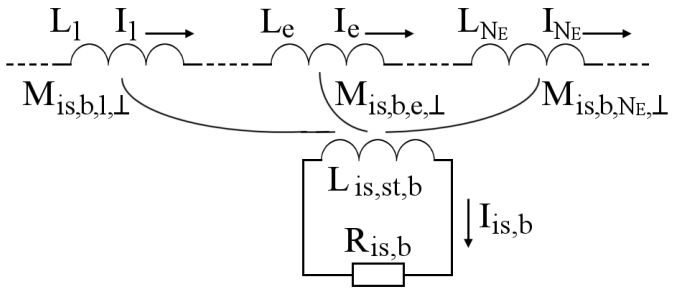

Figure 9: Equivalent LEDET sub-network modeling the inter-strand coupling currents in block b.

Finally, the total effect of local ISCC in a volume of conductor can be calculated. Consider a model block b composed of $N_{\mathrm{c,b}}$ conductors with length l_{b} [m]. Its total volume is $V_{\mathrm{c,b}} = N_{\mathrm{c,b}}\ wh\ l_{\mathrm{b}}$ [m^3]. By multiplying equation 55 by $N_{\mathrm{c,b}}\ l_{\mathrm{b}}$, a relation describing the coupling between the ISCC in block b and the currents in the electrical sub-network is obtained,

$$-R_{\mathrm{is,b}} I_{\mathrm{is,b}} = \sum_{e=1}^{N_{\mathrm{E}}} M_{\mathrm{is,b,e,\perp}} \frac{dI_{\mathrm{e}}}{dt} + L_{\mathrm{is,st,b}} \frac{dI_{\mathrm{is,b}}}{dt}, \qquad [\mathrm{V}] \quad (56)$$

where the equivalent resistance $R_{\mathrm{is,b}}$, self-inductance $L_{\mathrm{is,b}}$, and mutual inductances $M_{\mathrm{is,b,e,\perp}}$ of the ISCC loop representing the dynamic behavior of block b are defined as:

$$\begin{cases} R_{\mathrm{is,b}} = \dfrac{V_{\mathrm{c,b}}}{h^2} \dfrac{1}{\beta_{\mathrm{is,b}}} = \dfrac{w}{h} N_{\mathrm{c,b}}\ l_{\mathrm{b}} \dfrac{1}{\beta_{\mathrm{is,b}}} & [\Omega] \\ L_{\mathrm{is,st,b}} = \mu_0 \dfrac{V_{\mathrm{c,b}}}{h^2} = \mu_0 \dfrac{w}{h} N_{\mathrm{c,b}}\ l_{\mathrm{b}} & [\mathrm{H}] \\ M_{\mathrm{is,b,e,\perp}} = \dfrac{V_{\mathrm{c,b}}}{h} f_{\mathrm{b,e,\perp}} = w N_{\mathrm{c,b}} l_{\mathrm{b}} f_{\mathrm{b,e,\perp}} \qquad \text{for } e = 1...N_{\mathrm{E}}. & [\mathrm{H}] \end{cases} \quad (57)$$

Note the analogy between equations 56-57 and 29-30, derived for IFCC loops. The behavior of this simple system can be modeled by the equivalent lumped-element circuit shown in figure 9, composed of a closed loop of a resistor and a self-inductance coupled to the N_{E} self-inductances L_{e} present in the electrical sub-network.

In the case of a model block composed of a single non-stacked cable the equivalent inductance $L_{\mathrm{is,st,b}}$ in equation 56 is to be replaced by a more

appropriate

$$L_{\mathrm{is,c,b}} = \frac{\mu_0}{\pi}\left[\ln\left(\frac{w}{h}\right) + \frac{3}{2}\right] N_{\mathrm{c,b}}\ l_{\mathrm{b}}, \qquad [\mathrm{H}] \quad (58)$$

obtained multiplying equation 44 by $N_{\mathrm{c,b}}\ l_{\mathrm{b}}$.

In addition, the inter-strand coupling loss generated in the cable volume of a block b corresponds to the ohmic loss in the equivalent resistor $R_{\mathrm{is,b}}$,

$$P_{\mathrm{is,b}} = R_{\mathrm{is,b}} I^2_{\mathrm{is,b}}, \qquad [\mathrm{W}] \quad (59)$$

analogous to equation 31. This ISCL is used to solve the thermal balance in block b presented in equation 2.

The only unknown parameter in the model of equivalent ISCC loops is the contact resistance between two crossing strands R_{c}, inversely proportional to the ISCC time-constant and to the ISCL during transients at constant current-change.

The LEDET model of inter-filament and inter-strand coupling currents neglects the magnetic coupling between individual coupling loops, which could be included in the model with a radically different mathematical approach, based on FEM methods. However, this approximation greatly simplifies the problem and has significantly less influence on the system dynamics than other assumptions, such as uniformity of the physical properties along the direction of the conductor, and unknowns, such as material properties and magneto-resistivity.

5.3. Extension to other coupling-current mechanisms

More generally, also other coupling-current mechanisms can be simulated following a methodology analogous to that introduced in sections 5.1 and 5.2. The total generated loss and the effect of local currents on the magnet's differential self-inductance can be reproduced with a sub-network of lumped-elements.

In fact, a generic coupling-current mechanism characterized by a loss P_{cc} [W] and an equivalent coupling-current I_{cc} [A] is described by the following two relations:

$$\begin{cases} P_{\mathrm{cc}} = \beta_{\mathrm{cc}} V_{\mathrm{cc}} \left(\dfrac{dB_{\mathrm{cc}}}{dt}\right)^2 & [\mathrm{W}] \\ I_{\mathrm{cc}} = -\gamma_{\mathrm{cc}} \dfrac{dB_{\mathrm{cc}}}{dt}, & [\mathrm{A}] \end{cases} \quad (60)$$

plus a characteristic time constant, τ_{cc} [s], where V_{cc} [m^3] is the volume where the loss takes place, dB_{cc}/dt [Ts^{-1}] is the resulting total magnetic-field change, and β_{cc} [mΩ^{-1}] and γ_{cc} [m$^2\Omega^{-1}$] are characteristic parameters depending on the loss mechanism. The coupling between the local coupling currents and the currents in the main electrical circuit is described by the following equation:

$$-R_{cc}I_{cc} = \sum_{e=1}^{N_E} M_{cc,e}\frac{dI_e}{dt} + L_{cc}\frac{dI_{cc}}{dt}, \qquad [V] \quad (61)$$

where the equivalent resistance R_{cc}, self-inductance L_{cc}, and mutual inductances $M_{cc,e}$ of the generic coupling-current loop are defined as:

$$\begin{cases} R_{cc} = \dfrac{P_{cc}}{I_{cc}^2} = \dfrac{\beta_{cc}V_{cc}}{\gamma_{cc}^2} & [\Omega] \\ L_{cc} = \tau_{cc}R_{cc} = \dfrac{\tau_{cc}\beta_{cc}V_{cc}}{\gamma_{cc}^2} & [H] \\ M_{cc,e} = \dfrac{\beta_{cc}V_{cc}}{\gamma_{cc}}f_{cc,e} \qquad \text{for } e = 1...N_E, & [H] \end{cases} \quad (62)$$

where $f_{cc,e}$ [TA^{-1}] are N_E magnetic parameters characterizing the applied magnetic field B_a [T] generated by a current I_e [A] flowing through electrical element e. The definition of the above-mentioned parameters $M_{cc,e}$ is derived from the consideration that during a transient at constant ramp-rate the induced coupling currents do not vary (dI_{cc}/dt=0) and the local magnetic field-change coincides with the applied magnetic-field change (dB_{cc}/dt=dB_a/dt); hence, equation 61 is reduced to

$$\sum_{e=1}^{N_E} M_{cc,e}\frac{dI_e}{dt} = -R_{cc}I_{cc} = R_{cc}\gamma_{cc}\frac{dB_{cc}}{dt} = \frac{\beta_{cc}V_{cc}}{\gamma_{cc}}\sum_{e=1}^{N_E} f_{cc,e}\frac{dI_e}{dt}, \quad [V] \quad (63)$$

when the definition of $M_{cc,e}$ is found.

6. Conclusion

A new technique for modeling the behavior of a superconducting magnet called LEDET (Lumped-Element Dynamic Electro-Thermal) is developed, based on various coupled networks of lumped-elements. The energy-exchanges between different physical domains are correctly accounted

for, as well as the influence of local inter-filament and inter-strand coupling currents on the overall magnet differential self-inductance. The same simulation environment can simultaneously model macroscopic electrical transients and phenomena at the level of superconducting strands.

TALES (Transient Analysis with Lumped-Elements of Superconductors), a software based on this new technique, has been extensively validated against experimental results. Coupled electrical, magnetic, and thermal transients are successfully reproduced during and after magnet discharges obtained by triggering CLIQ, quench heaters, energy-extraction systems, or a combination of these. After its validation, the software allows deepening the understanding of the phenomena occurring in a superconducting magnet and of the influence of dynamic effects on the magnet's behavior.

The LEDET modeling technique proved a key ingredient for an effective implementation of the CLIQ technology, where very high current and magnetic-field changes are introduced in the various coil sections, and the effects of inter-filament coupling currents on the magnet's differential inductance is very significant. New CLIQ configurations can be analyzed to investigate their effectiveness on existing and future magnets of different geometries, sizes, types of superconductor, and strand and cable parameters.

[1] E. Ravaioli, *CLIQ*, PhD thesis University of Twente, The Netherlands, 2015, doi: 10.3990/1.9789036539081.

[2] H. De Gersem, C. Mühle, M. Clemens, G. Moritz, and T. Weiland, *Numerical Simulation of Eddy Currents in the Superconductive Rutherford Cable of a Fast-Pulsed Dipole Magnet*, Proceedings of the 6th European Conference on Applied Superconductivity (EUCAS 2003), September 2003.

[3] H. De Gersem and T. Weiland, *Finite-element models for superconductive cables with finite interwire resistance*, IEEE Transactions on Magnetics, vol. 40, no. 2, March 2004,doi: 10.1109/TMAG.2004.825454.

[4] S. Russenschuck, *Field Computation for Accelerator Magnets: Analytical and Numerical Methods for Electromagnetic Design and Optimization*, Hoboken, NJ, USA: Wiley, 2011.

[5] J. Kozak, *DIPOLE model in PSPICE*, CERN internal report, 2009.

[6] A. Laprade, S. Pearson, S. Benczkowski, G. Dolny, and F. Wheatley, *A New PSPICE Electro-Thermal Subcircuit For Power MOSFETs*, Application Note 7532 Fairchild, 2003.

[7] M.N. Wilson, *Superconducting Magnets*, Oxford University Press, Oxford, ISBN 0-019-854805-2, 1983.

[8] A.P. Verweij, *Electrodynamics of Superconducting Cables in Accelerator Magnets*, PhD thesis University of Twente, The Netherlands, 1995.

[9] G.H. Morgan, *Theoretical Behavior of Twisted Multicore Superconducting Wire in a TimeVarying Uniform Magnetic Field*, Journal of Applied Physics, vol. 41, no. 9, August 1970, doi: 10.1063/1.1659491.

[10] W.J. Jr. Carr, *AC loss in a twisted filamentary superconducting wire*, Journal of Applied Physics, vol. 45, no. 2, 1974.

[11] M. Maciejewski, *Automated, Object Oriented Simulation Framework for Superconducting Magnets Modelling at CERN*, Master's thesis University of Łodz, Poland, 2014.

[12] M. Maciejewski, E Ravaioli, B. Auchmann, A.P. Verweij, and A. Bartoszewicz, *Automated Lumped-Element Simulation Framework for Modelling of Transient Effects in Superconducting Magnets*, Proceedings of the 20th International Conference on Methods and Models in Automation and Robotics, 2015.

[13] E. Ravaioli, V.I. Datskov, C. Giloux, G. Kirby, H.H.J. ten Kate, and A.P. Verweij, *New, Coupling Loss Induced, Quench Protection System for Superconducting Accelerator Magnets*, IEEE Transactions on Applied Superconductivity, vol. 24, no. 3, June 2014, doi: 10.1109/TASC.2013.2281223.

[14] E. Ravaioli, V.I. Datskov, A.V. Dudarev, G. Kirby, K.A. Sperin, H.H.J. ten Kate, and A.P. Verweij, *First Experience with the New Coupling-Loss Induced Quench System*, Cryogenics, 2014, Vol. 60, pp. 33-43, http://dx.doi.org/10.1016/j.cryogenics.2014.01.008.

[15] E. Ravaioli, V.I. Datskov, G. Kirby, H.H.J. ten Kate, and A.P. Verweij, *A New Hybrid Protection System for High-Field Superconducting Magnets*, Superconductor Science and Technology, 2014, Vol. 27 (4), 044023, doi: 10.1088/0953-2048/27/4/044023.

[16] E. Ravaioli, V.I. Datskov, V. Desbiolles, J. Feuvrier, G. Kirby, M. Maciejewski, K.A. Sperin, H.H.J. ten Kate, A.P. Verweij, and G. Willering, *Towards an optimized Coupling-Loss Induced Quench protection system (CLIQ) for quadrupole magnets*, Physics Procedia, 2015, doi: 10.1016/j.phpro.2015.06.037.

[17] E. Ravaioli, H. Bajas, V.I. Datskov, V. Desbiolles, J. Feuvrier, G. Kirby, M. Maciejewski, G. Sabbi, H.H.J. ten Kate, and A.P. Verweij, *Protecting a Full-Scale Nb_3Sn Magnet with CLIQ, the New Coupling-Loss Induced Quench System*, IEEE Transactions on Applied Superconductivity, vol. 25, no. 3, June 2015, doi: 10.1109/TASC.2014.2364892.

[18] E. Ravaioli, H. Bajas, V.I. Datskov, J. Blomberg Ghini, G. Kirby, M. Maciejewski, H.H.J. ten Kate, A.P. Verweij, and G. Willering, *First implementation of the CLIQ quench protection system on a full-scale accelerator quadrupole magnet*, IEEE Transactions on Applied Superconductivity, 2015, to be published.

[19] E. Ravaioli, V.I. Datskov, G. Kirby, M. Maciejewski, H.H.J. ten Kate, and A.P. Verweij, *Advanced Quench Protection for the Nb_3Sn Quadrupoles for the High Luminosity LHC*, IEEE Transactions on Applied Superconductivity, 2015, to be published.

[20] E. Ravaioli, V.I. Datskov, G. Kirby, M. Maciejewski, H.H.J. ten Kate, A.P. Verweij, and G. Willering, *First implementation of the CLIQ quench protection system on a 14 m long full-scale LHC dipole magnet*, IEEE Transactions on Applied Superconductivity, 2015, to be published.

[21] E. Ravaioli, V.I. Datskov, J. Blomberg Ghini, G. Kirby, M. Maciejewski, G. Sabbi, H.H.J. ten Kate, and A.P. Verweij, *Quench protection of a 16 T block-coil dipole magnet for a 100 TeV Hadron Collider using CLIQ*, IEEE Transactions on Applied Superconductivity, 2015, to be published.

[22] E. Ravaioli, V.I. Datskov, G. Kirby, M. Maciejewski, H.H.J. ten Kate, and A.P. Verweij, *CLIQ-based quench protection of a chain of high-field superconducting magnets*, IEEE Transactions on Applied Superconductivity, 2015, to be published.

[23] B. Turck, *Coupling losses in various outer normal layers surrounding the filament bundle of a superconducting composite*, Journal of Applied Physics, vol. 50, no. 8, Aug 1979, doi: 10.1063/1.326641.

[24] B. Turck, *Effect of the respective positions of filament bundles and stabilizing copper on coupling losses in superconducting composites*, Cryogenics, vol. 22, 1982.

[25] S. Russenschuck, *ROXIE: Routine for the Optimization of Magnet X-Sections, Inverse Field Calculation and Coil End Design*, Ed. Geneva, Switzerland: CERN, April 1999.

[26] SOLENO. A high-precision magnetic field, inductances and forces calculation code for air-core systems of multi-solenoids developed by the applied superconductivity applications group at the University of Twente, Enschede, the Netherlands.

[27] L. Dresner, *Stability of Superconductors. Selected Topics in Superconductivity*, Springer US, 1995, ISBN 9780306450303.

[28] W.J. Jr. Carr, M.S. Walker, and J.H. Murphy, *Alternating field loss in a multifilament superconducting wire for weak ac fields superposed on a constant bias*, Journal of Applied Physics , vol. 46, no. 9, September 1975, doi: 10.1063/1.322108.

[29] M.S. Walker, J.H. Murphy, and W.J. Jr. Carr, *Alternating field losses in mixed matrix multifilament superconductors*, IEEE Transactions on Magnetics, vol. 11, no. 2, March 1975, doi: 10.1109/TMAG.1975.1058568.

[30] M.S. Walker, W.J. Jr. Carr, and J.H. Murphy, *Loss behavior in twisted filamentary superconductors*, IEEE Transactions on Magnetics, vol. 11, no. 5, September 1975, doi: 10.1109/TMAG.1975.1058849.

[31] *LHC design report*, CERN-2004-003, 2004.

[32] K.F. Goddard, A.A. Roy, and J.K. Sykulski, *Inductance and resistance calculations for a pair of rectangular conductors*, IEE Proceedings - Science, Measurement and Technology, vol. 152, no. 2, March 2005, doi: 10.1049/ip-smt:20041058.

[33] E.B. Rosa, *The Self and Mutual Inductances of Linear Conductors*, Bulletin of the Bureau of Standards 4 (2): 301344, 1908, doi: 10.6028/bulletin.088.